NANO LETTERS

pubs.acs.org/NanoLett

Electrokinetic Concentration of DNA Polymers in Nanofluidic Channels

Derek Stein,[†,‡] Zeno Deurvorst,[†] Frank H. J. van der Heyden,[†] Wiepke J. A. Koopmans,[†] Alan Gabel,[‡] and Cees Dekker*[,†]

[†]Kavli Institute of NanoScience, Delft University of Technology, Delft, The Netherlands, and [‡]Department of Physics, Brown University, Providence, Rhode Island 02912

ABSTRACT DNA molecules can be concentrated in a narrow region of a nanochannel when driven electrokinetically in submillimolar salt solutions. Transport experiments and theoretical modeling reveal the interplay of electrophoresis, electro-osmosis, and the unique statistical properties of confined polymers that lead to DNA aggregation. A finite conductance through the bulk of the device also plays a crucial role by influencing the electric fields in the nanochannel. We build on this understanding by demonstrating how a nanofluidic device with integrated electrodes can preconcentrate DNA at selected locations and at physiological salt concentrations that are relevant to lab-on-a-chip applications.

KEYWORDS Nanofluidic, DNA, electrokinetic, concentration

Miniature fluidic devices are having an important impact on biochemical diagnostic applications thanks to their ability to manipulate and analyze samples in extremely small quantities and at very high speeds.[1] Transport within "lab-on-a-chip" devices is commonly achieved using electrokinetic mechanisms: an applied electric field can drive a charged molecule relative to the fluid by electrophoresis, while the fluid itself can be dragged via the charged layer of counterions that accumulate near charged channel walls in a process known as electro-osmosis.[2−4] Electric fields can also drive more complex electrokinetic phenomena at short length scales, including induced charge electro-osmosis,[5,6] ac electro-osmosis,[7−10] concentration polarization,[11] and other electrokinetic phenomena.[12−14] The transport of analyte molecules, most notably long polymers like DNA, can be fundamentally altered in the nanofluidic regime, where their statistical properties grow increasingly important.[15−19] The interplay between electrokinetics and polymer physics that underlies DNA transport in nanochannels is nontrivial and can give rise to interesting behavior that remains poorly understood, despite the important role it may play in future nanofluidic technologies.[20,21]

In this Letter we focus on the concentration of long DNA molecules at a specific location in a nanofluidic channel by electrokinetic phenomena. Sample preconcentration plays an important role in lab-on-a-chip technology because chemical separations applications typically require a highly concentrated plug of analyte at the inlet, and methods to achieve this have attracted considerable interest.[15,22−29] Our attention was drawn to the possibility of all-electrokinetic DNA preconcentration by the observation of unusual electrically driven DNA flow patterns in silica nanochannels at low salt concentrations. At submillimolar ionic strengths, the application of an electric field caused DNA molecules to aggregate in a narrow band near one end of the channel, while molecules were depleted from the other end. This DNA aggregation phenomenon was not anticipated. However, it was intriguing because it might offer a practical approach to preconcentration if the location of the concentrated band could be controlled and if the strategy could be implemented at higher, biologically relevant salt concentrations. In this Letter, we show how electrokinetic DNA concentration can indeed be understood and controlled in nanofluidic channels.

We studied electrically driven DNA transport in thin, rectangular, slitlike nanochannels whose geometry is sketched in panels a and b in Figure 1. Standard optical lithography and etching methods defined thin, rectangular nanochannels in fused silica that were 4 mm long, that were 2−50 μm wide, and that were flanked by two rectangular, 1.5 mm wide slits, into which 1 mm diameter access holes had been milled. The channel height, h, was uniform across each device, including the wide rectangular slits, and was measured by step profilometry. The heights tested ranged from $h = 115$ nm to $h = 1$ μm. The nanochannels were sealed by bonding a patterned fused silica chip to a flat, 200 μm thick fused silica coverslip using a sodium silicate adhesion layer that was deposited from 2% aqueous solution by spinning at 5000 rpm. The full details of the bonding procedure have been described elsewhere.[30,31] The channels were filled with buffer solution and electrophoretically cleaned of ionic impurities by applying 50 V across the channel for ∼10 min. Electrokinetic transport was generated by applying a voltage V across the channel using silver electrodes inserted into opposing access holes.

We studied the transport of λ-DNA molecules (λ-DNA; Promega, Leiden, The Netherlands), which are 48502 base

* To whom correspondence should be addressed.
Received for review: 07/11/2009
Published on Web: 02/12/2010

DOI: 10.1021/nl902228p | *Nano Lett.* **2010,** *10,* 765–772

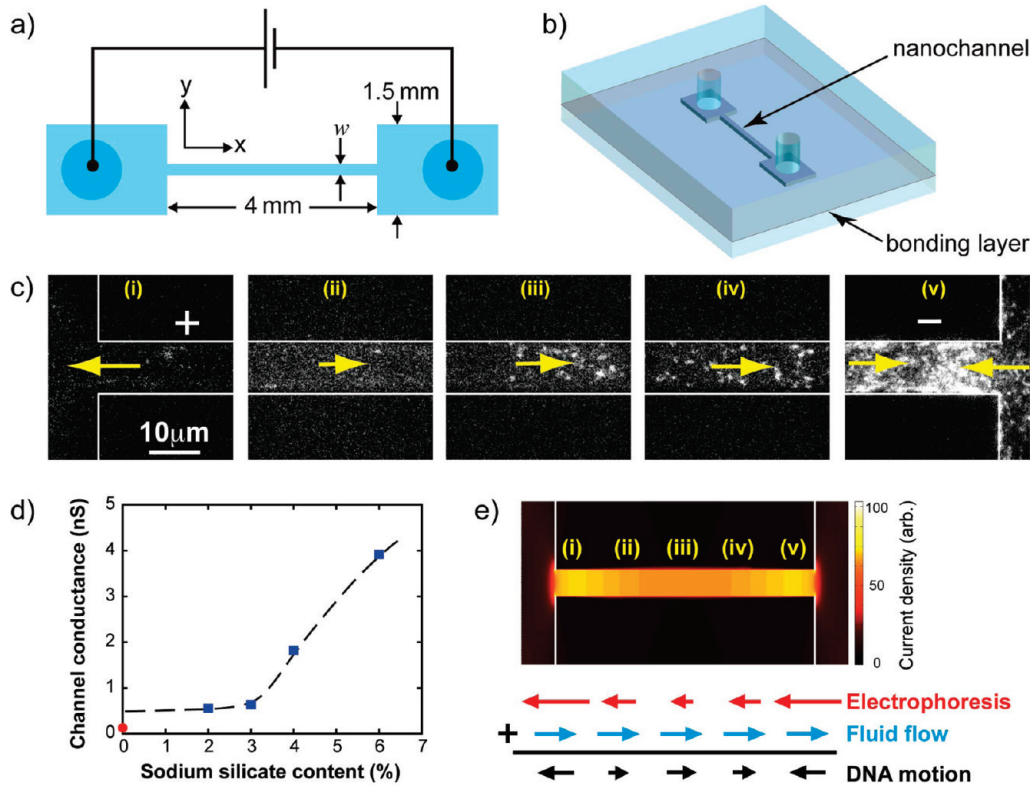

FIGURE 1. Electrokinetic DNA concentration in nanochannels. (a) Layout of the nanofluidic channel devices, as viewed from above. The light blue areas represent the thin regions, which include the narrow channel and the wide slits on either end, while the dark blue circles correspond to the deep access holes milled into the opposing slits. (b) A three-dimensional representation of the device. (c) Electrically driven DNA transport in a silica nanochannel under low salt conditions. Fluorescent micrographs of λ-DNA molecules were taken at five different locations along a 250 nm high channel 12 s after the application of 10 V and are arranged in a composite image. The KCl salt concentration was 0.25 mM. DNA concentrated near the channel entrance at the negative pole, and it depleted from the positive pole. The arrows indicate the velocity of DNA observed at different locations. (d) Ionic conductance in the sodium silicate bonding layer. The increasing conductances of 250 nm high channels filled with 0.25 mM KCl are plotted against the sodium silicate content in the bonding layer of the devices (blue squares). The dotted line is a guide to the eye. The red circle indicates the conductance of a device fabricated by thermal bonding, rather than silicate bonding. (e) Calculated current density distribution and schematic explanation of the DNA dynamics observed in part (c) caused by the finite conductivity of the bonding layer. The spatial variation of the current density across the channel, which is proportional to the electric field distribution, was calculated for a device as described in the text. Below, the red and blue arrows illustrate the electrophoretic and advective components of the DNA velocity, respectively, while the black arrow illustrates their net effect. Roman numerals indicate the corresponding locations in (a).

pairs long. The DNA was stained with fluorescent YOYO-1 dye (Molecular Probes, Eugene, OR) at a base-pair to dye ratio of 6:1, and was suspended in different salt solutions, prepared by diluting a stock buffer of 1 M KCl, 10 mM TRIS (pH = 8.0), 1 mM EDTA with water to their final salt concentrations. β-Mercaptoethanol (2% by volume) was added to prevent photobleaching. DNA was introduced into the nanochannels using a pressure-driven flow prior to the application of a voltage. In some experiments, suspensions of fluorescent carboxylate-modified 100 nm diameter beads (FluoSpheres; Invitrogen, Carlsbad, CA) were used as tracer particles instead of DNA. The dynamics of the DNA molecules and the beads were recorded by epifluorescence optical miscroscopy using an electron multiplication CCD camera (Andor, Belfast, Northern Ireland) combined with an inverted oil-immersion fluorescence microscope (100×, 1.4 N.A.; Olympus, Tokyo, Japan) focused at the channel midplane.

Under high salt conditions (10 mM, 50 mM, 150 mM, and 1 M), the electrically driven transport of DNA we observed in our nanochannels was as anticipated: DNA moved continuously from the positive pole toward the negative pole, at a constant velocity along the length of the narrow channel, and at reduced speeds in the wide rectangular slits. The fact that DNA molecules, which are negatively charged at pH = 8, moved toward the negative pole simply indicated the dominance of electro-osmosis over electrophoresis in our channels, as will be discussed.

At sub-millimolar salt concentrations, however, we observed DNA dynamics that departed qualitatively from the anticipated, high salt behavior. The noteworthy features of the flow patterns are depicted in the fluorescent images shown in Figure 1c, corresponding to an $h = 250$ nm, 10 μm wide channel filled with 0.25 mM KCl buffer (see also movie 1, Supporting Information). When 10 V was applied across the device, DNA near the positive pole was driven out

DOI: 10.1021/nl902228p | *Nano Lett.* **2010,** *10,* 765–772

of the channel toward that positive pole. DNA initially located near the center of the channel, however, traveled in the opposite direction—toward the negative pole—before being arrested at a concentration point close to the exit point to the wide rectangular slit at the negative pole. DNA initially in the wide slit at the negative pole traveled toward the positive pole, before being arrested at the same concentration point. The striking feature of this transport behavior was that the velocity of DNA flipped sign twice along the length of the channel, resulting in the concentration point where the DNA aggregated, and a region near the opposite end of the channel from which DNA became completely depleted.

We observed qualitatively similar flow patterns at submillimolar salt concentrations for all channel heights tested (h = 115 nm, 250 nm, 500 nm, 750 nm, and 1 μm for 50 μm wide channels) and for all channel widths (2, 10, 20, and 50 μm). The location at which the DNA concentrated always occurred was near the negative channel entrance but tended to migrate slowly outward (toward the negative pole) over time. Consequently, a salient and consistent feature of the low-salt behavior was the formation of a growing semicircular band of concentrated DNA about the channel entrance (Figure 3a; see also movie 2, Supporting Information). The speed at which the concentrated band of DNA shifted outward increased with applied voltage (see Supporting Information, SI.B). However, the speed of migration was always much slower than the typical speeds of DNA molecules outside the concentrated band at each applied voltage.

What caused such dramatic DNA dynamics to emerge at low salt concentrations? We suspected that the small but finite conductance through the bulk of the fluidic device significantly influenced the electric field distribution in the channel. Two observations hinted at this. First, as noted, no DNA concentration or depletion was observed in the high salt concentration range (10 mM to 1 M), where the high conductivity of the fluid should overwhelm any conductance through the silica or the silicate bonding layer of the device. Only at low salt concentrations, where the fluid conductivity was also low, did the DNA concentration occur. Second, the low-salt DNA dynamics pointed to conductivity through the device: DNA was electrically driven directly onto the inner boundary of the slit at the negative pole, which implied a nonzero current density across the channel boundary and therefore a finite conductivity of the material.[32]

Before exploring the implications of a finite device conductivity on the electrokinetic transport of DNA, we first consider an important alternative explanation for the observed concentration phenomenon. Dielectrophoresis has been used to concentrate polarizable analytes, including DNA, in microfluidic devices with lateral constrictions.[33−35] The dielectrophoretic force arises from the coupling between electric field gradients and the induced dipole moment of a polarizable object. Although dielectrophoretic trapping is normally achieved using alternating fields for which the electrophoretic and electro-osmotic forces average to zero, the dielectrophoretic force is present even under constant applied fields, as in our experiments. In order to conclusively exclude the possibility that dielectrophoresis drove the DNA concentration phenomenon reported here, we performed theoretical analyses and control experiments presented in the Supporting Information. The estimated strength of the dielectrophoretic force was always at least 2 orders of magnitude weaker than the electrophoretic force in our experiments (Supporting Information SI.A), while the influence of the voltage (Supporting Information SI.B) and the geometry of the channel entrance (Supporting Information SI.C) on the transport of DNA were also inconsistent with the dielectrophoresis hypothesis.

An explanation for the electrokinetic concentration of DNA we observed instead lies in the electrical properties of our devices. We confirmed that an electrical conduction path existed through the sodium silicate bonding layer that held the fluidic devices together by measuring the conductances of 100 μm wide, 250 nm high channel devices prepared with increasing amounts of sodium silicate bonding material and filled with 0.25 mM KCl solutions (Figure 1d). The conductivity of devices clearly increased with silicate content and provided evidence for a finite contribution to the conductance by the silicate layer used in our DNA transport experiments, which was deposited from 2 % silicate solution. We also tested the electrically driven dynamics of DNA in a 200 nm high channel that had been made by a thermal bonding procedure (Micronit Microfluidics, Netherlands), which requires no sodium silicate and is expected to have better insulating properties. In these thermally bonded channels, DNA concentration did not occur for the 0−50 V range of applied voltages tested, even at the lowest salt concentration of 0.25 mM (although modest time variations in the velocities were observed). The conductance of a 100 μm wide, thermally bonded channel is also shown in Figure 1d (red dot). The low value likely resulted from a combination of improved bonding, and a reduced surface charge density in the surface-charge-governed ion transport regime[30] caused by high-temperature bonding.[36]

Numerical simulations of the current density in the nanochannel show the strong influence that the measured conductivity of the bonding layer has on electrical transport (Figure 2c). The sheet conductivity of the bonding layer was assumed to be 10 % of the ionic conductivity integrated over the channel height. This value was consistent with the experimentally determined values of the low-salt channel conductivity presented in Figure 2b: The excess conductance of a 2 % silicate bonding layer was estimated after extrapolating the measured channel conductance data to 0 %. Our simulations reveal that the electric current density clearly decreased in the center of a channel relative to the two ends. (Details of the numerical simulations can be found in the Supporting Information, section SI.D.)

The dramatic DNA dynamics observed at low salt concentrations can thus be explained by the competition be-

DOI: 10.1021/nl902228p | *Nano Lett.* **2010,** *10,* 765−772

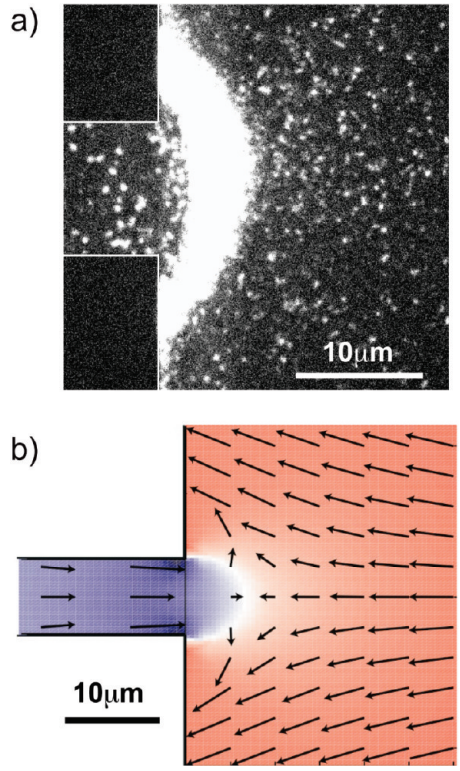

FIGURE 2. DNA transport simulations. (a) A fluorescence micrograph of DNA accumulation near the negative entrance of a 500 nm-high channel caused by the application of a 2 V potential for 120 s. The concentrated DNA formed the white, semicircular band around the entrance of the nanochannel. (b) The results of a simple DNA transport model (see text) predict DNA flow patterns that match the velocities observed in (a) well. The arrows depict the local velocity. DNA is predicted to converge on the concentrated band, where there is a stagnation point at the "top" midpoint along the arc.

tween electrophoresis and advection. As sketched in Figure 1e, the net DNA velocity in the nanochannel is the sum of two components: (1) electrophoresis, whereby the negatively charged DNA travels toward the positive pole at a velocity $\vec{v}_{\text{elec}} = \mu\vec{E}$ relative to the fluid, where μ is the electrophoretic mobility in an electric field $\vec{E}$; and (2) advection, whereby electro-osmotic motion of the fluid in the negatively charged silica nanochannel drags the DNA toward the negative pole at a velocity $\vec{v}_{\text{advect}}$. Since the electrically driven current density weakens in the center of the nanochannel, so does $\vec{v}_{\text{elec}}$. On the other hand, the fluid is incompressible and cannot permeate the channel boundaries, so the volume rate of fluid displacement across any section of the channel must be constant, and $\vec{v}_{\text{advect}}$ does not vary along the channel. Figure 1e shows that this picture captures the most important features of the observed flow patterns. Near the ends of the channel, electrophoresis dominates, driving DNA toward the positive pole. Near the center of the channel, the advection of DNA dominates, carrying molecules toward the negative pole. The lengthwise component of DNA velocity therefore flips the sign twice, as observed, resulting in regions of strong DNA concentration and depletion near the negative and positive channel entrances, respectively.

The slow, outward motion of the concentrated band of DNA is likely the result of a higher order transport effect. This can be surmised from the fact that the speed of individual DNA molecules toward the concentrated band always greatly exceeded the speed at which the band itself would migrate. We speculate that the presence of a high concentration of DNA in one region of the channel, and its depletion elsewhere, might influence the zeta potential along the length of the channel, resulting in band migration as the electro-osmotic flow term slowly grows. The transport of ions into the bonding layer might also alter the conductivity of that layer over time. A more detailed study would be required, however, to properly understand the phenomenon.

Our explanation of the observed DNA dynamics has been mostly qualitative so far. We now present a simple quantitative model that predicts the observed electrically driven flow patterns of DNA with surprising accuracy. We begin with the fluid dynamics. The small scale of a micro- or nanofluidic device ensures that fluid flow is in the linear, low-Reynolds-number regime described by incompressible Stokes flow

$$\eta\nabla^2 u - \vec{\nabla}p = \vec{0} \tag{1}$$

$$\vec{\nabla}\cdot u = 0 \tag{2}$$

where η is the fluid viscosity, p is the pressure, and $\vec{u}$ is the fluid flow velocity, whose normal component must vanish at the channel walls. The application of an electric field drives electro-osmotic fluid flow (EOF), whose velocity profile across the channel height is pluglike (flat). In the limit of thin double layers (the Debye length $\lambda_D \ll h$), EOF can be described by imposing a slip condition at the surfaces[37]

$$u_{\text{slip}} = -\varepsilon\varepsilon_0\zeta\eta^{-1}E\Big|_{\text{surface}} \tag{3}$$

where ζ is the zeta potential. This description offers a reasonable approximation of our experiments, even though the low salt concentrations tested correspond to Debye lengths close to 20 nm. Both EOF and $\vec{v}_{\text{elec}}$ are driven by applied electric fields, which satisfy Laplace's equation

$$\nabla^2 E = \vec{0} \tag{4}$$

In our experiments, the channel height and surface properties (i.e., ζ) of the nanochannels were nominally uniform, and no pressure difference was applied. Under these conditions, $\vec{u}$ and $\vec{E}$ are governed by identical equations inside the channel (eq 1 and eq 4, respectively). It is

DOI: 10.1021/nl902228p | *Nano Lett.* **2010,** *10,* 765–772

instead through different boundary conditions that we distinguish the low- and high-salt transport behavior. For high salt concentrations, where the electrical conductivity of the channel walls was negligible relative to that of the fluid, neither the fluid nor the electrical current could penetrate the channel perimeter. Therefore $\vec{v}_{elec} \propto \vec{v}_{advect}$, and the lengthwise component of $\vec{v}_{DNA}$ is predicted to point in the same direction across the entire nanochannel, just as was observed. At low salt concentrations, however, electrical conduction through the channel material can no longer be neglected. Ionic currents permeate the boundary of the nanochannel, whereas the fluid cannot. Consequently, the symmetry between fluid flow and ionic current flow is broken.

We tested this simple but quantitative transport model by simulating the net DNA dynamics in our channels at low salt. To do this, we numerically computed $\vec{v}_{elec}$ and $\vec{v}_{advect}$ independently and then summed them (details of the simulation are described in the Supporting Information, section SI.E). We simplified the calculations by ignoring variations in the electric field and the fluid flow across the nanochannel height, instead treating the geometry as a thin, two-dimensional sheet. The sheet conductivity of the silicate bonding layer was the same value as used in the calculation of electric field distributions presented in Figure 1e, for which we found experimental support. The only adjustable parameter in our model was the dimensionless quantity, $\alpha \equiv \mu\eta/\varepsilon\varepsilon_0\zeta$, corresponding to the ratio of the electrophoretic mobility to the electro-osmotic mobility. We used $\alpha = 0.9$, a value consistent with the known electrophoretic mobility of DNA and the zeta potential of silica under the conditions of our experiments.[38,39] Figure 2 shows that our simple model accurately captured the most striking feature of the DNA dynamics, which was the concentration of DNA near the negative channel entrance.

Several interesting aspects of electrokinetic DNA transport in our nanochannels merit further consideration. First is remarkable how well the preceding model fared, considering how it completely ignored variations in the fluid velocity across the height of the nanochannel. In fact, significant recirculating fluid flows are expected to occur, explicitly requiring fluid motion in the vertical direction, and tending to disperse DNA hydrodynamically. The aggregation of DNA in narrow bands is therefore remarkable in itself, as we now discuss. When the electric field varies along a long, uniform channel, it leads to a corresponding variation of the fluid slip velocity according to eq 3. This situation was treated analytically for slab geometries.[40] It was found that recirculating flows of an incompressible fluid are generated inside a channel because when fluid is driven into slower or oppositely moving fluid along the surface of the channel, it must recirculate through the center. The rolling flows induced by an oscillating slip velocity have been experimentally observed in patterned PDMS channels.[41] Similarly, we observed 100 nm diameter fluorescent beads moving past

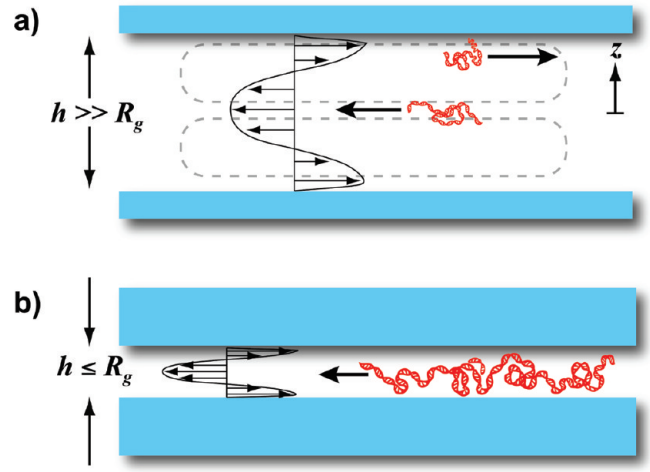

FIGURE 3. Schematic of DNA transport regimes. Cross-sectional views of two fluidic channels are depicted in which recirculating fluid flow profiles are illustrated. (a) When the channel height is large compared with the size of the polymer coil, the velocity of a molecule depends on its height, *z*, in the channel. (b) The transport of a polymer is predicted to become *z*-independent in the nanoconfined regime where the channel height is smaller than the polymer coil size.

each other in opposite directions near the negative entrance of our nanochannels at low salt, indicating that the beads were caught in recirculating flows.[42] DNA molecules, on the other hand, became highly concentrated in the same region of the nanochannels.

The special properties of nanoconfined polymers[18,19] must be considered to properly understand electrokinetic DNA transport in nanochannels. We argue that statistical phenomena are what allow DNA to become highly concentrated, exhibiting qualitatively different behavior as compared with rigid beads. To illustrate, note that since $\vec{v}_{advect}$ results from a complex fluid velocity profile that can include recirculating flows, two DNA molecules located the same distance along a channel could travel at different speeds, and even in opposite directions, by sitting at different heights within a recirculating flow, as sketched in Figure 3a. Such a situation would arise in channels that are high compared with the molecular coil size, $2R_g$ (where the radius of gyration, $R_g \approx 0.73$ μm in our experiments). However, in nanochannels that are thin compared with$2R_g$, a random-flight polymer adopts conformations that distribute its contour over the entire height of the channel, as sketched in Figure 3b. The many segments of a polymer simultaneously sample all parts of the flow. Consequently, DNA transport in nanochannels becomes effectively two-dimensional, as $\vec{v}_{DNA}$ is the average of the local segment velocities over the channel height.[18] Nanoconfined polymers thus suppress hydrodynamic dispersion, explaining why DNA can aggregate, even in the presence of recirculating flows.

We have analyzed the interplay between recirculating fluid flows and the equilibrium statistics of nanoconfined polymers analytically. Details of this analysis are presented in the Supporting Information, section SI.F. Briefly, to

DOI: 10.1021/nl902228p | *Nano Lett.* **2010,** *10,* 765–772

determine the advective component of the DNA velocity, $\vec{v}_{\text{advect}}$, we made use of the average distribution of DNA segments across the channel height derived by Casassa[43,44] and Ajdari's expression for the recirculating fluid velocity profile induced by a sinusoidal modulation of the electro-osmotic slip velocity in an infinite slab geometry.[40] We are interested in the motion of DNA in an electric field that varies arbitrarily in the lengthwise direction, which can be expressed as

$$\vec{E}(x) = \vec{E}_0 + \sum_q \vec{E}_q \sin(qx)$$

where $\vec{E}_q$ is the amplitude corresponding to the wavenumber q. Combining $\vec{v}_{\text{advect}}$ with $\vec{v}_{\text{elec}}$, we derived the following expression for $\vec{v}_{\text{DNA}}$

$$v_{\text{DNA}}(x) \cong \left(\mu - \frac{\varepsilon\varepsilon_0\zeta}{\eta}\right)E_0 + \left(\mu + 0.7\frac{\varepsilon\varepsilon_0\zeta}{\eta}\right)\sum_q E_q \sin(qx) \tag{5}$$

The first term in eq 5 corresponds to DNA motion in a uniform electric field that generates pure pluglike fluid flow. The second term accounts for the sinusoidal electric field components that generate recirculating flows. The modulations in $\vec{v}_{\text{DNA}}$ are clearly proportional to those in $\vec{E}$. These results support the simplified picture we used to explain the DNA concentration phenomenon in Figure 1e and reveal why the simple two-dimensional calculations used to predict the flows in Figure 3 were so successful: Variations in the electric field lead to corresponding variations in the velocity of DNA, which can indeed flip sign along the nanochannel.

The quasi-two-dimensional picture of electrokinetic DNA transport presented here is based on equilibrium polymer configurations. The validity of this assumption requires the polymer relaxation rate to be fast compared with the fluid shear rate, i.e., for low Weissenberg numbers. A simple estimate shows that this condition has a wide range of applicability in nanofluidics: Hsieh et al.[45] pointed out that the relevant relaxation time for a confined polymer is the Zimm time,[46] τ_z, of a confined polymer "blob", for which $R_g \approx h/2$ within de Gennes' scaling model.[47] The blob relaxation rate is $1/\tau_z$, where $\tau_z \approx 0.05\eta h^3/k_B T$. This rate is compared with the fluid shear rate, $\dot{\gamma}$, which scales as the ratio of the electro-osmotic velocity to the channel height, $\dot{\gamma} \approx \varepsilon\varepsilon_0\zeta\vec{E}/\eta h$. As the height of a fluidic channel is reduced, the polymer relaxation rate increases faster than the shear rate. Equilibrium polymer statistics therefore remain valid in nanochannels up to high values of the driving field. For example, we estimate the breakdown will occur at electric fields above ~100 V/cm in a $h = 250$ nm silica channel,[39] which is higher than that used in normal electrophoresis applications and higher than that used in our experiments.

We applied our electrokinetic DNA transport model by designing a simple nanofluidic DNA preconcentration device (Figure 4). This device was intended to demonstrate two things: first, that significant predictions of our theoretical model could be verified by an experimental test; second, that we could control DNA dynamics by inducing DNA preconcentration at a desired location and at ionic strengths high enough to be relevant for bioanalytical applications.

The preconcentration device consisted of a 250 nm high, 30 μm wide channel fabricated across two connected but electrically floating 20 μm wide gold electrodes, as sketched in Figure 4a. The lithographically patterned electrodes were spaced 2 mm apart from one another and were embedded in the bottom chip of the fluidic device so as not to disturb the nanochannel cross section. The purpose of the electrodes was to permit Faradaic reactions at the surface and thereby maintain a constant electrochemical potential in the region between them. A potential applied across the access holes should therefore have the following effects: Electric fields should be generated in the outer sections of the channel, where DNA electrophoresis toward the positive pole should dominate advection. In the middle section, where we expect the electric fields to be canceled, only advection should remain, transporting DNA toward the negative pole. We consequently predicted DNA preconcentration to occur at the electrode near the negative pole and depletion at the other electrode. Importantly, this behavior was predicted for all salt concentrations, including the high concentrations at which no DNA aggregation occurred previously.

Figure 4 shows the DNA dynamics that were observed in the nanofluidic preconcentrator filled with 50 mM KCl buffer after the application of 10 V. DNA molecules that were initially located on either side of the electrode near the positive pole all moved away from that electrode, the predicted site of DNA depletion (see also movie 3 in the Supporting Information). At the other electrode, the applied potential drew DNA in from either side. The DNA concentrated in a ~10 μm band whose location was within micrometers of the predicted electrode (see also movie 4 in the Supporting Information). These observations agreed extremely well with our predictions.

The operation of the preconcentrator device reinforced our basic understanding about electrokinetic DNA transport in nanochannels. It also illustrated how integrated electrodes can induce dramatic yet controllable effects on DNA dynamics in fluidic devices. Engineering the aggregation of DNA molecules (or other biopolymers) at the inlet of a separation device is of practical relevance. The all-electrokinetic technique reported here is distinct from existing methods that concentrate DNA at a physical barrier, such as a porous plug[26,29] or a nanofabricated entropic barrier,[24] and from field-amplified sample stacking,[27,28,48] which relies on an interface between regions of fluid of different conductivity. Our preconcentrator shared some important similarities with an electrophoretic focusing device reported by Huang and Ivory, in which an array of electrodes was used to generate an electric field gradient in a microchannel.[22]

DOI: 10.1021/nl902228p | *Nano Lett.* **2010,** *10,* 765–772

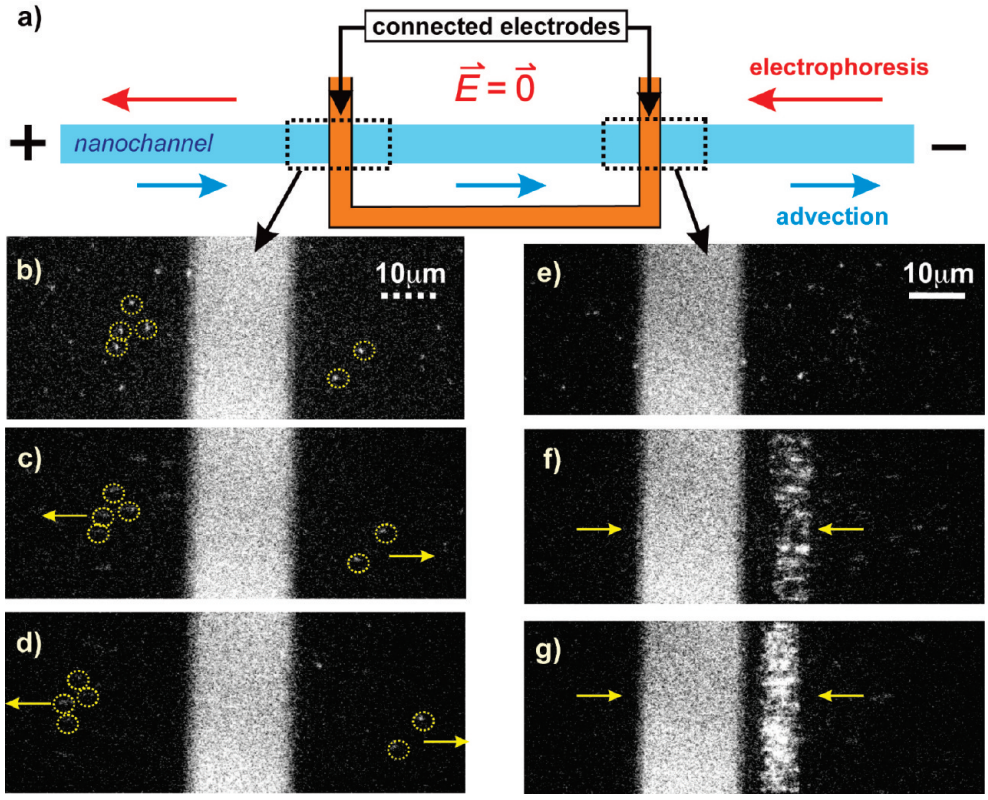

FIGURE 4. Inducing controlled DNA concentration and depletion in a 500 nm high nanofluidic channel at high salt concentration using integrated electrodes. (a) Top view schematic of the device. The channel is illustrated, showing connected, floating electrodes that cancel the electric field between them. The red and blue arrows indicate the expected effects of electrophoresis and advection on the DNA velocity in the different regions of the channel, respectively. Fluorescent micrographs show DNA molecules near the electrode at the positive pole (b) prior to the application of 10 V across the channel and then at increasing times thereafter (c and d). The same molecules are circled in each micrograph to highlight their motion away from that electrode. Near the electrode at the negative pole, DNA molecules (e) prior to the application of 10 V and (f, g) shortly thereafter show a clear concentration of DNA within a ~10 μm band.

However, the Huang device countered the electrophoretic motion of proteins with a pressure-driven flow, and it did not take advantage of the dispersion-suppressing properties of nanoconfined polymers, in contrast with our all-electrokinetic approach. This last difference is the most significant, as it can explain why we observed DNA aggregating in a ~10 μm wide band, rather than the ~0.5 mm wide bands of protein achieved in the absence of strong polymer confinement.

In conclusion, we have demonstrated how the electrokinetic transport of DNA in a nanochannel can result in regions of strong concentration and depletion. Transport is determined by the competition between electrophoresis and advection in electro-osmotically driven fluid flows. The properties of confined polymers also play an important role. The distribution of DNA segments across a nanochannel render the dynamics effectively two-dimensional, which makes it possible for DNA to accumulate within a tiny volume despite the presence of recirculating flows. A predictive model that incorporates all these effects has been verified, and the applicability of this approach to controlling DNA dynamics in a nanofluidic device has been demonstrated. The use of integrated electrodes to cancel electric fields over a section of a channel reveals a simple means of achieving high degrees of DNA sample preconcentration, which is a key requirement for many chemical separation applications. Since an arbitrary pattern of electrodes can be incorporated into a nanofluidic device by lithography, and then actuated by applying voltages to them, the potential exists to achieve electrical control over molecular transport for more sophisticated "lab-on-a-chip" applications.

Supporting Information Available. Additional information on numerical modeling of ionic conductance in a nanochannel, simulations of electrokinetic DNA transport in a nanochannel at low salt, and analytical expression for $\vec{v}_{DNA}$ in the presence of recirculating flows and four videos that illustrate flow patterns. This material is available free of charge via the Internet at http://pubs.acs.org.

REFERENCES AND NOTES

(1) Whitesides, G. M. *Nature* **2006**, *442*, 368–373.
(2) Stone, H. A.; Stroock, A. D.; Ajdari, A. *Annu. Rev. Fluid Mech.* **2004**, *36*, 381–411.
(3) Squires, T. M.; Quake, S. R. *Rev. Mod. Phys.* **2005**, *77*, 977–1026.
(4) Hunter, R. J. *Foundations of colloid science*; Oxford University Press: Oxford and New York, 2001.
(5) Bazant, M. Z.; Squires, T. M. *Phys. Rev. Lett.* **2004**, *92*, No. 066101.

DOI: 10.1021/nl902228p | *Nano Lett.* **2010,** *10,* 765–772

(6) Levitan, J. A.; Devasenathipathy, S.; Studer, V.; Ben, Y. X.; Thorsen, T.; Squires, T. M.; Bazant, M. Z. *Colloids Surf., A* **2005**, *267*, 122–132.
(7) Ramos, A.; Morgan, H.; Green, N. G.; Castellanos, A. *J. Colloid Interface Sci.* **1999**, *217*, 420–422.
(8) Urbanski, J. P.; Thorsen, T.; Levitan, J. A.; Bazant, M. Z. *Appl. Phys. Lett.* **2006**, *89*, 143508.
(9) Storey, B. D.; Edwards, L. R.; Kilic, M. S.; Bazant, M. Z. *Phys Rev E* **2008**, *77*, No. 036317.
(10) Studer, V.; Pepin, A.; Chen, Y.; Ajdari, A. *Analyst* **2004**, *129*, 944–949.
(11) Kim, S. J.; Wang, Y. C.; Lee, J. H.; Jang, H.; Han, J. *Phys. Rev. Lett.* **2007**, *99*, No. 044501.
(12) Rubinstein, I.; Zaltzman, B.; Kedem, O. *J. Membr. Sci.* **1997**, *125*, 17–21.
(13) Yossifon, G.; Chang, H. C. *Phys. Rev. Lett.* **2008**, *101*, 254501.
(14) Rubinstein, I.; Zaltzman, B.; Lerman, I. *Phys. Rev. E* **2005**, *72*, No. 011505.
(15) Volkmuth, W. D.; Austin, R. H. *Nature* **1992**, *358*, 600–602.
(16) Bakajin, O. B.; Duke, T. A. J.; Chou, C. F.; Chan, S. S.; Austin, R. H.; Cox, E. C. *Phys. Rev. Lett.* **1998**, *80*, 2737–2740.
(17) Han, J.; Turner, S. W.; Craighead, H. G. *Phys. Rev. Lett.* **1999**, *83*, 1688–1691.
(18) Stein, D.; van der Heyden, F. H. J.; Koopmans, W. J. A.; Dekker, C. *Proc. Natl. Acad. Sci. U.S.A.* **2006**, *103*, 15853–15858.
(19) Hsieh, C. C.; Doyle, P. S. *Korea–Aust. Rheol. J.* **2008**, *20*, 127–142.
(20) Pennathur, S.; Baldessari, F.; Santiago, J. G.; Kattah, M. G.; Steinman, J. B.; Utz, P. J. *Anal. Chem.* **2007**, *79*, 8316–8322.
(21) Craighead, H. *Nature* **2006**, *442*, 387–393.
(22) Huang, Z.; Ivory, C. F. *Anal. Chem.* **1999**, *71*, 1628–1632.
(23) Han, J.; Craighead, H. G. *Science* **2000**, *288*, 1026–1029.
(24) Wang, Y. C.; Stevens, A. L.; Han, J. Y. *Anal. Chem.* **2005**, *77*, 4293–4299.
(25) Foote, R. S.; Khandurina, J.; Jacobson, S. C.; Ramsey, J. M. *Anal. Chem.* **2005**, *77*, 57–63.
(26) Khandurina, J.; Jacobson, S. C.; Waters, L. C.; Foote, R. S.; Ramsey, J. M. *Anal. Chem.* **1999**, *71*, 1815–1819.
(27) Lichtenberg, J.; Verpoorte, E.; de Rooij, N. F. *Electrophoresis* **2001**, *22*, 258–271.
(28) Jung, B.; Bharadwaj, R.; Santiago, J. G. *Electrophoresis* **2003**, *24*, 3476–3483.
(29) Wang, Q. G.; Yue, B. F.; Lee, M. L. *J. Chromatogr., Sect. A* **2004**, *1025*, 139–146.
(30) Stein, D.; Kruithof, M.; Dekker, C. *Phys. Rev. Lett.* **2004**, *93*, No. 035901.
(31) Wang, H. Y.; Foote, R. S.; Jacobson, S. C.; Schneibel, J. H.; Ramsey, J. M. *Sens. Actuators, B* **1997**, *45*, 199–207.
(32) We note that this observation could not be explained by variations in the zeta potential across the device. We therefore exclude inhomogeneities in the surface potential as a possible explanation for the low-salt DNA aggregation phenomenon.
(33) Chou, C. F.; Tegenfeldt, J. O.; Bakajin, O.; Chan, S. S.; Cox, E. C.; Darnton, N.; Duke, T.; Austin, R. H. *Biophys. J.* **2002**, *83*, 2170–2179.
(34) Cummings, E. B.; Singh, A. K. *Anal. Chem.* **2003**, *75*, 4724–4731.
(35) Lapizco-Encinas, B. H.; Simmons, B. A.; Cummings, E. B.; Fintschenko, Y. *Anal. Chem.* **2004**, *76*, 1571–1579.
(36) Iler, R. K. *The chemistry of silica: solubility, polymerization, colloid and surface properties, and biochemistry*; Wiley: New York, 1979.
(37) Anderson, J. L. *Annu. Rev. Fluid Mech.* **1989**, *21*, 61–99.
(38) Stellwagen, N. C.; Gelfi, C.; Righetti, P. G. *Biopolymers* **1997**, *42*, 687–703.
(39) Sze, A.; Erickson, D.; Ren, L.; Li, D. *J. Colloid Interface Sci.* **2003**, *261*, 402–410.
(40) Ajdari, A. *Phys. Rev. E* **1996**, *53*, 4996–5005.
(41) Stroock, A. D.; Weck, M.; Chiu, D. T.; Huck, W. T. S.; Kenis, P. J. A.; Ismagilov, R. F.; Whitesides, G. M. *Phys. Rev. Lett.* **2001**, *86*, 6050–6050.
(42) Lettieri, G. L.; Dodge, A.; Boer, G.; de Rooij, N. F.; Verpoorte, E. *Lab Chip* **2003**, *3*, 34–39.
(43) Casassa, E. F. *J. Polym. Sci., Part B: Polym. Lett.* **1967**, *5*, 773–778.
(44) Casassa, E. F.; Tagami, Y. *Macromolecules* **1969**, *2*, 14–26.
(45) Hsieh, C. C.; Balducci, A.; Doyle, P. S. *Macromolecules* **2007**, *40*, 5196–5205.
(46) Doi, M.; Edwards, S. F. *The Theory of Polymer Dynamics*; Oxford University Press: Oxford, 1986.
(47) de Gennes P.-G. *Scaling concepts in polymer physics*; Cornell University Press: Ithaca, NY, 1979.
(48) Jacobson, S. C.; Ramsey, J. M. *Electrophoresis* **1995**, *16*, 481–486.

DOI: 10.1021/nl902228p | *Nano Lett.* **2010,** *10,* 765–772